

Large-Scale Weather Regimes and Local Climate Over the Western United States

Andrew W. Robertson and Michael Ghil

Department of Atmospheric Sciences
and Institute of Geophysics and Planetary Physics,
University of California, Los Angeles, Los Angeles, CA

January 14, 1998

J. Climate, submitted

Correspondence address:

Dr. Andrew W. Robertson
Department of Atmospheric Sciences
UCLA
405 Hilgard Avenue
Los Angeles, CA 90095-1565
Tel: (310) 825 1038
Fax: (310) 206 5219
E-mail: andy@atmos.ucla.edu

Abstract

Weather regimes are used to determine changes in the statistical distribution of winter precipitation and temperature at eight locations within the western United States. Six regimes are identified from daily 700-mb heights during 46 winters (1949–95) over the North Pacific sector applying cluster analysis; these include the Pacific-North American (PNA) pattern, reverse-PNA, and a Pacific Ω -block. Most of the regimes are shown to have a statistically significant effect on the local median temperature, as well as daily temperature extremes, with differences between locations being secondary. Local precipitation frequency is also conditioned significantly by certain weather regimes, but differences between groups of locations are larger. Precipitation extremes are dispersed and hard to classify.

The extent to which the El Niño-Southern Oscillation (ENSO) modulates the probability of occurrence of each of the six weather regimes is then investigated. Warm-event (El Niño) winters are found to be associated with a significant increase in prevalence of a PNA-like regime, in which negative height anomalies exhibit a northwest-southeast tilt over the North Pacific. During La Niña winters, this PNA-like regime occurs significantly less frequently, while a regime characterized by a ridge over southwestern North America becomes more prevalent. These two regimes are associated with opposing regional precipitation-frequency anomalies that contribute to a north-south contrast in precipitation anomalies over the western United States during El Niño and La Niña winters.

1. Introduction

It is becoming increasingly well established that atmospheric intraseasonal variability is characterized by certain large-scale flow patterns that appear repeatedly at fixed geographical locations, and persist beyond the life time of individual synoptic-scale storms. These patterns were termed *Grosswetterlagen* by Bauer (1951), and have since been systematized in terms of *teleconnection patterns* (Wallace and Gutzler, 1981), or *persistent anomalies* (Dole and Gordon, 1983) in mid-tropospheric height fields. They are characterized by an approximately equivalent-barotropic vertical structure (Blackmon et al., 1979). More recently, the concept of *weather regimes* (Rheinhold and Pierrehumbert, 1982) or *planetary flow regimes* (Legras and Ghil, 1985) has been introduced in attempting to connect the observations of persistent and recurring patterns with synoptic-scale or planetary-scale atmospheric dynamics. Regimes have been defined in terms of clustering, fuzzy (Mo and Ghil, 1988) or hierarchical (Cheng and Wallace, 1993), maxima in the probability density function (PDF) of the large-scale low-frequency flow (Molteni et al. 1990; Kimoto and Ghil, 1993a, b), or by quasi-stationarity (Ghil and Childress, 1987, Sec. 6.4; Vautard, 1990). Regimes typically persist for several days to two weeks, with rapid transitions between them associated with the nonlinearity of atmospheric dynamics; a Markov chain of transition probabilities describes well their predictability (Mo and Ghil, 1988; Vautard et al. 1990; Kimoto and Ghil, 1993b).

Weather regimes are known to organize midlatitude storms (e.g. Robertson and Metz, 1990), and to be associated with significant temperature anomalies (Michelangeli et al., 1995). By inference, they affect local weather. On the other hand, there is evidence from observations and general circulation model (GCM) experiments that the distribution of weather regimes over the North Pacific in a given winter is affected by the El Niño-Southern Oscillation (ENSO; cf. Horel and Mechoso, 1988; Molteni et al., 1993).

In addition to converging observational evidence, theoretical studies indicate that flow regimes can be associated with important regularities of the large-scale atmosphere's attractor, either as multiple stable equilibria, representing the totality of the attractor (Charney and DeVore, 1979; Benzi et al., 1984), or as unstable equilibria and limit cycles embedded in a strange attractor (Legras and Ghil, 1985; Vautard and Legras, 1988; Kimoto and Ghil, 1993b). The sensitivity of weather regimes to small perturbations has important implications for medium-range weather forecasting (Miyakoda et al., 1983; Tibaldi and Molteni, 1990; Corti and Palmer, 1997). Using the Legras and Ghil (1985) model (Ghil and Childress, 1987, Sec. 6.5), the three-component Lorenz model (Molteni et al., 1993), or the observations (Kimoto, 1989), it has been argued that external forcings on midlatitudes, associated with ENSO or anthropogenic effects, may affect systematically the PDF of weather regimes.

Hydrological models for surface water supply, hydroelectric power production and agricultural production require as input local precipitation and temperature on a *daily* basis. Statistical models that relate these to large-scale weather types have been constructed by Bardossy and Plate (1992) based on a classification scheme traditionally used by the Deutscher Wetterdienst (German weather service). To identify the weather types most related to daily precipitation, investigators have used empirical orthogonal function (EOF) analyses of daily 700-mb geopotential heights (Dettinger and Cayan, 1992) or sea-level pressure together with 850-mb temperature and geopotential heights (Wilson et al., 1992). Classification and regression tree (CART) analysis was used by Hughes et al. (1993) and Zorita et al. (1995). These latter studies seek optimal statistical “downscaling” relationships between the large-scale circulation and local daily conditions, without the benefit of any prior information on the phase-space structure of the large scales. Weather regimes provide a dynamical paradigm for characterizing the multimodal statistics of the planetary-scale

climate system, and thus provide a natural point of departure for a downscaling method to local daily precipitation and temperature, i.e., regional climate.

The aim of this paper is to investigate the extent to which dynamically defined weather regimes determine the statistics of daily precipitation and temperature over the western United States in winter. This is the season in which weather regimes are most extensively documented, and the one in which the region receives the bulk of its water supply. We also investigate the extent to which ENSO affects the distribution of weather regimes itself. ENSO is known to affect ultimately, precipitation and temperatures over the western United States in winter, and particularly the hydrologic extremes (Ropelewski and Halpert, 1987, 1996; Cayan and Webb, 1992), although the extent and systematic character of this influence have been a matter of debate (Namias and Cayan, 1984; Mo et al., 1991; Dettinger et al., 1995; Gershunov and Barnett, 1997).

The paper is organized as follows. Section 2 describes the data sets used, large-scale and local. In section 3, we construct conventional correlation maps to paint a broad-brush picture of the relationship between large and regional scales. Kimoto and Ghil (1993b) found that over the wintertime North Pacific, about 50% of days in a 37-year observed data set of 700-mb height maps fell into distinct flow regimes; these weather regimes are constructed in section 4 for our 46-winter (1949 to 1995) data set. In section 5, we stratify daily regional statistics by regime. Interannual relationships between tropical sea surface temperatures (SST) and weather regime recurrence are examined in section 6, with the conclusions summarized in section 7.

2. Data sets

Two data sets are used, one for each of the two spatial scales of interest. For the large scale, we analyze the National Centers for Environmental Prediction (NCEP; formerly NMC) twice-daily time series of 700-mb heights for 46 winters, December

1949–February 1995. The data are provided on a diamond grid (two shifted regular 10° -grids) over the Northern Hemisphere, from which we select the North-Pacific–North-American sector (120°E – 60°W , 20°N – 70°N). Some grid points north of 55°N are omitted following Barnston and Livezey (1987), to obtain an approximately uniform-area grid of 184 points. To identify weather regimes, daily averages are formed for the $N=46\times 90=4140$ days and the data are low-pass filtered with a half-power point at 10 days. The mean seasonal cycle is subtracted on a daily basis from the low-pass filtered data set. The number of independent degrees-of-freedom in the time series is estimated as $N/\tau \approx 520$ with $\tau \approx 8$ days equal to the decorrelation time of the leading principal component of the deseasonalized filtered data set.

The regional data set consists of daily precipitation totals together with daily temperature maxima and minima for eight regions within the western United States, kindly provided by D. Cayan and L. Riddle. Each regional time series consists of an average over 4–6 stations, constructed with the methodology described by Aguado et al. (1992). For the daily time series used here, 365 daily means and standard deviations were used in place of the 12 monthly values used by Aguado and co-authors (L. Riddle, 1997, pers. commun.). Daily averages of temperature are formed from the daily maxima and minima. The geographical locations of the stations that comprise each regional time series are given in Fig. 1 and Table 1. The eight time series span three broad geographical regions of the western United States: (a) Carson-Truckee and the Central Sierra, in the Sierra Nevada of California, (b) Western Washington and the Yellowstone River in the Pacific Northwest and northwestern interior respectively, and (c) the Rio Grande and Gunnison, Salt and Virgin Rivers in the southwestern interior (mostly within the Four Corners states).

[Fig. 1 and Table 1 near here, please.]

3. Correlation maps

To get an overall picture of the relationship between large and regional scales on interannual time scales, Figs. 2 and 3 show maps of the cross-correlations between the interannual variability of winter (DJF) means of 700-mb height on the one hand, and regional temperature and precipitation, respectively. Maps for three selected regions, from the Yellowstone River in the north to the Salt River in the south, are displayed in panels (a)–(c) of each figure.

[Figs. 2 and 3 near here, please.]

Large-scale interannual fluctuations of geopotential height appear to accompany local variations of both precipitation and especially temperature, but the correlation patterns differ. Temperature exhibits very large-scale negative cross-correlations with 700-mb heights over the entire North Pacific, for all three regions (Figs. 2a–c). The local cross-correlations are positive, since 700-mb height reflects lower-tropospheric thickness—and thus surface-air temperature—when the vertical structure is equivalent barotropic. The largest correlations, however, are the negative ones upstream over the Pacific, and all three patterns broadly resemble the Pacific-North American (PNA) teleconnection pattern (Wallace and Gutzler, 1981). Excess winter precipitation is correlated locally with below-average geopotential heights, but the largest cross-correlation values for the Central Sierra and Salt River occur far away, off the West Coast (Fig. 3b, c). Sizable and coherent correlations occur upstream over the Pacific for the Yellowstone River as well (Fig. 3a), but the correlation patterns differ substantially from one region to another in the case of local precipitation.

4. Weather regimes

There is no unique or optimal way of classifying weather regimes, so we use two independent methods, based on pattern recurrence, to construct them: the PDF bump-hunting method of Fukunaga and Hostetler (1975), as used by Kimoto and Ghil (1993b; KG hereafter) and the dynamical clustering (or K -means) method (MacQueen, 1967), as used by Michelangeli et al. (1995; MVL hereafter). The PDF method defines a regime in terms of the state vectors of maps—or points in the large-scale atmosphere’s phase space—which lie in the vicinity of a PDF maximum, so that only a subset of the days is classified into regimes. The K -means method is a *partitioning method* that classifies *all* days into a predefined number of clusters such as to minimize the sum of squared distances within the set of clusters (e.g., Anderson, 1958).

Both methods were applied to the 46-winter data set of 700-mb height maps for the North-Pacific–North-American sector prepared as described in section 2. The application was carried out as explained by KG, in a subspace given by the leading EOFs. The latter are defined as the eigenvectors of the correlation matrix, which was found to yield slightly more regimes using the PDF bump-hunting method than does the covariance matrix (six vs. four, see below). The bump-hunting method was coded independently, following the methodology of KG. An IMSL (1991) library program was used to implement the K -means method, with an initial 10% subset of points used to determine the initial seeds, and the clustering repeated 50 times to eliminate any sensitivity to initial seeds (cf. MVL).

Bump hunting on the PDF in the subspace of the leading four EOFs yielded six regimes. Following KG, we used an angular metric and a smoothing parameter of $h=40^\circ$ to compute the Epanechnikov kernel to estimate the PDF from the daily data set. Points within a radius of $r=30^\circ$ in solid angle of the peaks in the PDF were selected to define the clusters, which thus have a regular conical shape (see Mo and Ghil, 1988). This choice of r gives negligible overlap between clusters and assigns 26% of the total 4140 days to one of

them. In the angular metric, the cosine of the solid angle between points corresponds to the pattern correlation between the daily maps in physical space (Mo and Ghil, 1988); thus all daily maps within a given cluster have a pattern correlation of $\cos(30^\circ)=0.866$ or greater with the central map.

As in KG, an automatic bump-hunting technique—via the “mean-shift” algorithm of Fukunaga and Hostetler (1975)—was used to locate peaks in the PDF, starting from local maxima on the chronological trajectory. A chronological local maximum is defined in each successive 10-day segment of the time series if the daily map at the PDF maximum in that segment has a pattern correlation of less than 0.4 with the preceding local maximum so defined (KG). To determine the appropriate h , its value was varied between 30° and 45° , and a range identified in which the number of clusters is insensitive to changes in h .

Figure 4 shows composite hemispheric maps of daily low-pass filtered height anomalies for the six PDF regimes. With the exception of Regime 1, all have close counterparts in the seven regimes identified by KG using the same methodology—see Table 2. Regimes 2 and 4 are the familiar PNA and reverse PNA (RNA), respectively, and closely resemble opposite phases of the one-point correlation maps of Wallace and Gutzler (1981). The subtle asymmetry between regimes 2 and 4 was already identified by Dole (1986) in his study of persistent atmospheric anomalies over the Pacific. The western Pacific teleconnection pattern of Wallace and Gutzler (1981) does not appear, perhaps due to our particular choice of sector.

[Fig. 4 and Table 2 near here, please.]

The three Pacific regimes identified by MVL are a subset of our six regimes (see Table 2). The comparison becomes very close if the covariance matrix is used to define the leading-EOF subspace, in which case only 4 clusters are obtained with $h=40^\circ$ (not shown). This smaller number of clusters is more consistent with MVL, who argue from a Monte

Carlo test against red noise that only 3 clusters can be isolated from the observed record over the North Pacific (see also Smyth et al., 1997, for a detailed discussion of this point). Repeating the K -means analysis for $K=4$ in the subspace of the 10 leading covariance EOFs, and $K=6$ using the 10 leading correlation EOFs, yields regime composite maps (not shown) in close correspondence with the PDF regimes in both cases. For $K=6$, the pattern correlations of each PDF-regime in Fig. 4 with its K -means counterpart are: 0.94, 0.92, 0.63, 0.85, 0.95, and 0.98 respectively. The agreement in pattern is very close in most cases, despite the fact that the K -means method was intentionally applied in an EOF subspace of higher dimension; these higher-order EOFs evidently contribute but little. The level of agreement is quite remarkable, given that the six PDF regimes account for only 26% of days, while all days are classified by the K -means method.

Larger clusters can be obtained using the PDF bump-hunting method by increasing their radius r , but only at the expense of overlapping clusters. Hannachi and Legras (1995) have circumvented this problem by relaxing the requirement that the clusters have regular conical shape. They used a simulated annealing method to allow irregular boundaries, based on solving a traveling salesman problem (TSP; Press et al., 1992). The TSP finds, iteratively, the shortest closed path between “cities”, which in this case are the points in the EOF state space defined by the daily 700-mb height maps. We have applied the TSP to assign non-classified days to their nearest cluster, using the clusters in Fig. 4 as our point of departure. All remaining days can be classified in this way, but we choose to assign only daily maps within an angular distance of 60° (i.e., a pattern correlation of 0.5) of the cluster centroids. The resulting regime-composites have pattern correlations of 0.986 or greater with those in Fig. 4, and contain 491, 361, 361, 300, 275, and 309 days respectively, making up a total of 2097 or 51% of the 4140 daily maps.

5. Regional statistics

The weather regime patterns in Fig. 4 are sign-definite, but are broadly consistent with the linear correlation maps in Figs. 2 and 3. From a regime perspective, warmer winters in the central Sierra Nevada, for example, appear from Fig. 2 to be characterized by above-normal prevalence of a PNA-like pattern. We now quantify the relationship between the weather regimes and local precipitation and temperature in each region.

In this section and the next, we use the regimes derived using the PDF bump-hunting method with conical clusters (Fig. 4), unless stated otherwise. All the computations have been repeated using the larger clusters obtained with both simulated annealing (51% of maps classified) and the *K*-means method (100% classified). In each case, the results and their statistical significance are qualitatively very similar to those shown. The magnitudes of the regional anomalies are generally smaller in the latter two cases because the clusters are larger (not shown).

The distribution of daily temperature is approximately normal (Dettinger and Cayan, 1992). For each weather regime in turn, we compare the median and the two tails of the distribution of daily temperature with those defined by the full 46-winter record. The relative frequency of days warmer than the local winter median temperature for each weather regime is plotted in Fig. 5. For example, a frequency change of +40% means that days warmer than the climatological median occur 40% more often in the subset of days belonging to that regime, than the expected 50%. The error bars show the 95% confidence limits, derived using a simple reshuffling Monte Carlo (“bootstrap”) procedure with 1000 shuffles. Deviations in the frequency of warmer-than-median days are generally statistically significant at all localities for most regimes.

[Fig. 5 near here, please.]

The principal regime dependence of the number of warm days is between regimes characterized by blocked flow over the North Pacific with a trough over the western United States (Regimes 3, 4, 5), and regimes with zonal anomalies over the Pacific with a downstream ridge (Regimes 1, 2, 6). The latter contain more warmer days than average, and the former less. Regimes 2 and 4 constitute opposite phases of the PNA, and the large temperature difference at most stations between them is consistent with the correlation patterns in Fig. 2. The largest regime deviations in median temperature are in the Sierra Nevada and the Pacific Northwest.

Deviations in the frequency of temperature extremes, defined by the 10%-tails of the daily maximum or minimum temperature distributions are plotted in Fig. 6. The differences in daily temperature extremes are generally much larger than those in central tendency (note different scales on the ordinate). Both are generally in the same sense as for the median, with some exceptions. Changes in the cold tail tend to be larger than those in the warm tail in the Sierra Nevada. Despite the much smaller sample sizes, most of the deviations in the tails of the temperature distribution are also statistically significant. Regional differences are more marked in the distribution tails: Regime 5 (Ω -block) is associated with more extremely cold days in Western Washington, the Yellowstone River regions and in the Southwest, while Regime 4 (the RNA) is most often associated with extreme cold in the Sierra Nevada.

[Fig. 6 near here, please.]

Daily precipitation has a one-tailed distribution that is well approximated by the gamma distribution (Dettinger and Cayan, 1992). We focus first on the number of days with recorded precipitation, and then consider the tail of the distribution. Differences in the frequency of wet days between each regime and climatology are displayed in Fig. 7. The regime-dependence of precipitation frequency is slightly less clear-cut than for temperature,

with fewer results that are statistically significant. However, the PNA regime (# 2) is significantly drier at almost all localities, while its “reverse”, the RNA (# 4) is significantly wetter; the exceptions—Salt River for PNA and Western Washington for RNA—have precipitation anomalies of the same sign as the other locations, only less significant. The other “blocked” regimes (# 3, 5) tend to be wetter in the Southwest as well. Regimes 1 and 6 (associated preferentially with El Niño and La Niña respectively, see below) also show frequency anomalies of different signs by region. Regime 6 is significantly drier in the south but wetter in the north. Regime 1 is significantly wetter in the Sierra Nevada and parts of the Southwest, but drier at the Yellowstone River. Very similar results are obtained if the frequency of days with greater than 2.5mm of precipitation is considered (not shown).

[Fig. 7 near here, please.]

Heavy precipitation events are defined here as having daily totals that exceed the 75th percentile of days with measurable precipitation. Changes in the frequency are generally not statistically significant. Only about 1–2 regimes per location lead to heavy-precipitation days that are significantly more or less frequent than for the entire data set, at the 95% level or nearly so (not shown). In contrast to temperature extremes, regime deviations in heavy-precipitation frequency are in general no larger than those of precipitation frequency itself. Only in Western Washington do three out of the six regimes show significant deviations in heavy precipitation. Here, Regime 6 is associated with more frequent heavy precipitation events. In the southwest, by contrast, Regime 5 tends to be associated with heavy precipitation (not shown).

Since only about a quarter of days are classified into regimes by the PDF bump-hunting method, year-to-year changes in local temperature or precipitation anomalies are not necessarily accounted for fully by changes in weather-regime frequency. To check the

extent to which the local winter anomalies are determined by regime-frequency changes, regime frequencies were computed for anomalous winters in each of the eight regions, defined as local winter-averaged anomalies—in temperature or precipitation frequency—of greater than one standard deviation. Again a simple bootstrapping scheme was used to estimate statistical significance, in which the winters were reshuffled 100 times prior to calculating the statistics. Figure 8 illustrates the differences in frequency between warm and cold winters (circles), and wet and dry winters (diamonds), using the *K*-means regimes. The error bars indicate the 90% confidence interval. Similar results were obtained using the PDF method, but the levels of significance were generally below the 90% level.

[Fig. 8 near here, please.]

Overall, the correspondence is good between regimes which are significantly associated with anomalous local weather on a daily basis (Figs. 5 and 7) and those whose frequency of occurrence changes during anomalous winters (Fig. 8). The statistical significance of the latter is somewhat lower—for reasons associated with lower sample size—and the main feature is the contrast between winters dominated by the PNA (Regime 2) compared to the reverse PNA (Regime 4). At most stations throughout the western United States, winters with a high recurrence of the PNA regime tend to be warm and dry; the opposite is the case for the RNA. The contrast is most statistically significant for the Central Sierra and Virgin River time series.

6. Relationships with tropical SST

It is well known that the extratropical circulation over the North Pacific is affected by warm (El Niño) and cold (La Niña) events in the eastern tropical Pacific (e.g., Horel and Wallace, 1981; Kumar and Hoerling 1997). Kimoto (1989) has demonstrated that the distribution of certain sectorial weather regimes (see KG) is biased according to the phase of the Southern Oscillation index (SOI), with a weak but statistically significant preference

toward the PNA for negative SOI values (El Niño). Similar results have been obtained from GCM experiments (Horel and Mechoso, 1988; Brankovic et al., 1994).

Figure 9 illustrates the regime frequencies during El Niño and La Niña winters; these are defined here by excursions of the standardized SOI, averaged over the respective winter, that exceed 1.0 in absolute value: positive for La Niña ($\text{SOI} > 1.0$), and negative for El Niño ($\text{SOI} < -1.0$). The error bars denote the 95% significance level, based on 1000 random reshufflings. The most significant deviations in regime frequency are associated with Regime 1, which is significantly more prevalent during El Niño winters, and less prevalent during La Niña. Regime 6 is significantly less prevalent during El Niño winters, and tends to be more prevalent during La Niña. By contrast, the PNA (Regime 2) and RNA (Regime 4) show only weak changes in frequency, and then only during La Niña winters. Similar results are obtained if a 0.5 threshold is used for the standardized SOI, or if simulated annealing or the *K*-means regime definitions are used.

[Fig. 9 near here, please.]

Composite SST anomalies for the winters with regime frequencies above the 80th percentile are plotted in Fig. 10, giving a sample of 10–12 winters for each regime. Again, very similar patterns were obtained using regimes derived by simulated annealing or the *K*-means method. Regime 1 is associated with SST anomalies in both the tropical and North Pacific that are the hallmark of El Niño. We have corroborated this relationship using a joint multichannel singular spectrum analysis (Kimoto et al., 1991; Plaut and Vautard, 1994) of SST and 700-mb geopotential height data over the Pacific sector. During the El Niño phase of the joint analysis, as expressed by the SST anomalies, the height pattern closely resembles Regime 1 (not shown). These results are consistent with the studies of Horel and Mechoso (1988) and Deser and Blackmon (1995), who found North Pacific height anomalies associated with El Niño and the El Niño-minus-La Niña difference

respectively, to exhibit a northwest-southeast tilt over the North Pacific, and thus to differ from the PNA pattern. Regime 6 is associated with statistically significant composite SST anomalies in the eastern equatorial Pacific characteristic of La Niña: these are weaker than in the El Niño case, which is consistent with the smaller statistical significance of these regimes' frequency difference in Fig. 9, and with a nonlinearity in the weather regimes' response to ENSO. Again, the association of the PNA and RNA with opposite ENSO phases is much weaker than that of Regimes 1 and 6.

[Fig. 10 near here, please.]

The PNA and RNA (Regimes 2 and 4) are associated with SST anomalies over the central and eastern North Pacific of opposite signs, but only a small-to-moderate fraction of the anomalies' spatial pattern is statistically significant. These anomalies can be interpreted qualitatively in terms of the latent heat flux anomalies that accompany the most frequently occurring weather regimes (Cayan, 1992).

7. Summary and discussion

We have investigated (i) the extent to which the daily distributions of temperature and precipitation at eight localities in the western United States (see Fig. 1) are controlled by weather regimes over the North-Pacific–North-American sector during winter, and (ii) how much these regimes themselves depend on the phase of ENSO. One-point correlation maps between 700-mb geopotential height fields averaged over the 3-month winter (DJF) for a 46-winter period, on the one hand, and local temperature and precipitation time series in the western United States (Figs. 2 and 3), on the other, both show strong correlations, locally as well as remotely, over the North Pacific. Local correlations are positive for temperature and negative for precipitation. Sizable and coherent remote correlations occur upstream in both cases; the temperature correlations show strong projections onto the PNA pattern, while the precipitation correlation patterns appear more subtle. The correlation

patterns vary as one moves southward from the Yellowstone River to the Salt River, especially in the case of precipitation.

Two independent methods of defining weather regimes were applied to low-pass filtered winter geopotential heights over the North-Pacific–North-American sector; the PDF bump-hunting method (KG) and the *K*-means method (MVL). The resulting daily composites (Fig. 3) are remarkably similar, given that the PDF classifies only 26% of days as belonging to a regime, whereas by definition all days are classified by the *K*-means method. The regimes include the well known PNA and RNA patterns (Wallace and Gutzler, 1981; Dole and Gordon, 1983) as well as further patterns identified by previous authors (Table 2). Broadly speaking, the regimes fall into two categories: those with a trough over the North Pacific and a ridge downstream over western North America (Regimes 1, 2, and 6), and vice versa (Regimes 3, 4, and 5). These two broad categories correspond to the sectorial results of Cheng and Wallace (1993) and of Smyth et al. (1997).

Daily temperature and precipitation measurements in the eight regions were partitioned into subsets according to the weather regime. Local distributions for each subset were compared with the full set of $N=46\times 90=4140$ winter days, with statistical significance estimated by reshuffling the days 1000 times. Regime deviations in median temperature are generally significant at the 95% level for all regimes, except Regime 1, in all eight regions (Fig. 5). Deviations in the warm and cold tails correspond with some exceptions to those in the median (Fig. 6). There are fewer significant deviations in precipitation frequency (Fig. 7), and deviations in the tail of the local precipitation distributions are generally not significant. The main dependencies of local temperature (Figs. 5 and 6) and precipitation (Fig. 7) on weather regime are:

- The PNA and RNA (Regimes 2 and 4, respectively) are associated with the largest temporal contrasts in local temperature and precipitation; the PNA tends to yield warm and dry weather in almost all eight regions, while the RNA is cold and wet.
- Blocked-flow regimes over the North Pacific with a trough downstream over the Rocky Mountains (Regimes 3, 4, and 5) are on average colder than the zonal regimes (1, 2, and 6) at most localities. The blocked regimes tend to be wetter in the south.
- Region-to-region variations are most marked in the tails of the temperature distribution: Regime 5 (Ω -block) is associated with a much larger number of extremely cold days in Western Washington and the Yellowstone River regions than anywhere else, while Regime 4 (the RNA) is much more often associated with extreme cold in the Sierra Nevada.

Interannual anomalies in temperature and precipitation-frequency for the various locations are generally found to be associated with interannual changes in weather-regime frequency (Fig. 8). In cases where the large-scale regimes can be identified unequivocally with a tendency for wetness or dryness at a given location, wet years do in most cases differ significantly from dry years in terms of the frequency of the corresponding regimes. The same is true for temperature. Due to the small extent of the data set in hand, these conclusions only hold when using the *K*-means regime classification method; the PDF regimes contain too few days to allow interannual anomalies at most locations to be characterized with high statistical significance.

Since interannual anomalies in local temperature and precipitation can be partially characterized in terms of changes in weather-regime frequency, we have investigated how the latter are related to ENSO. Both in terms of its frequency during low- versus high-SOI winters (Fig. 9), and SST anomalies in the tropical Pacific during winters in which the regime occurs most frequently (Fig. 10). In terms of the six regimes identified (Fig. 4),

ENSO is characterized by an anomalously high frequency of Regime 1 during El Niño winters, and a relative absence of this regime during La Niña. To a smaller extent, Regime 6 is less frequent during El Niño winters and more prevalent during La Niña. On the other hand, the PNA and RNA (Regimes 2 and 4) show only a weak association with ENSO. Our results suggest that the teleconnections associated with ENSO over the North-Pacific–North American sector during winter are largely due to the anomalous frequency of Regime 1, rather than a linear response characterized by the PNA and RNA.

In terms of temperature, the regional effects of Regime 1 are always weaker than those associated with the PNA. Both tend to yield relatively warm weather across the western United States, but Regime 1 is only significantly warmer in the north, with fewer cold extremes across the entire western United States. In terms of precipitation frequency, Regimes 1 and 2 are generally characterized by anomalies of opposite sign. Regime 1 (the one associated with El Niño) is significantly wetter in the Sierra Nevada and the Southwest, and significantly drier at the Yellowstone River in the north. Regime 2 is significantly drier in almost all 8 regions.

Regime 6 tends to be more strongly associated with La Niña than the RNA (Regime 4), both in terms of SOI values and SST anomalies, although the association is somewhat weaker than for Regime 1 with El Niño (Figs. 9 and 10). Regime 6 tends to result in significantly warmer weather throughout the West, and is drier in the Southwest and wetter in the Northwest. It thus contrasts with Regime 1, whose frequency-of-occurrence is enhanced by El Niño and which is wetter in the Sierra Nevada and the Southwest, but drier at the Yellowstone River. Regimes 1 and 6 may thus contribute to the north-south contrast in precipitation over western North America during ENSO events found by previous authors (e.g. Cayan and Webb, 1992).

The relationships between weather regimes and regional weather, on the one hand, and these regimes and ENSO, on the other, were derived for six specific regimes. However, the qualitative nature and statistical significance of these relationships is not limited too severely by the methodology used in the classification. Our results showed little sensitivity to including as little as one quarter of all maps, when using KG's PDF bump-hunting method, as many as all maps, when using MVL's K -means method, or about half the maps, when using Hannachi and Legras' (1995) simulated annealing in defining the regimes. Likewise, the results showed little sensitivity to the size and way of defining the subspace in which the classification was carried out. We can hope, therefore, that the present results are fairly robust and insensitive to the exact choice of blocked and zonal regimes over the North-Pacific–North-American sector.

Acknowledgments. It is a pleasure to thank D. Cayan, M. Dettinger, and M. Kimoto for fruitful discussions. We are especially grateful to D. Cayan and L. Riddle for providing the regional data, M. Dettinger for supplying the geopotential height data, and to S. Koo for coding the K -means clustering algorithm. This work was supported by the University of California's Campus-Laboratory Collaboration (CLC) program, and by NASA Grant NAG 5-713.

References

- Aguado, E., D. Cayan, L. Riddle, and M. Roos, 1992: Climatic fluctuations and the timing of West Coast streamflow. *J. Climate*, **5**, 1468-1483.
- Anderson, T. W., 1958: *An Introduction to Multivariate Statistical Analysis*. John Wiley and Sons Inc., New York.
- Bardossy, A., and E. J. Plate, 1992: Space-time model for daily rainfall using atmospheric circulation patterns. *Water Resour. Res.*, **28**, 1247-1259.
- Barnston, A. G., and R. E. Livezey, 1987: Classification, seasonality and persistence of low-frequency atmospheric circulation patterns. *Mon. Wea. Rev.*, **115**, 1083-1126.
- Bauer, F., 1951: Extended range weather forecasting. *Compendium of Meteorology*. American Meteorological Society, 814-833.
- Bengtsson, L., K. Arpe, E. Roeckner, and U. Schulzweida, 1996: Climate predictability experiments with a general circulation model. *Climate Dynamics*, **12**, 261-278.
- Benzi, R., P. Malguzzi, A. Speranza, and A. Sutera, 1986: The statistical properties of general atmospheric circulation: Observational evidence and a minimal theory of bimodality. *Quart. J. Met. Soc.*, **112**, 661-674.
- Blackmon, M. L., R. A. Madden, J. M. Wallace, and D. S. Gutzler, 1979: Geographical variations in the vertical structure of geopotential height fluctuations. *J. Atmos. Sci.*, **36**, 2450-2466.
- Brankovic, C., T. N. Palmer, and L. Ferranti, 1994: Predictability of seasonal atmospheric variations. *J. Climate*, **7**, 217-237.

- Cayan, D. R. 1992. Latent and sensible heat flux anomalies over the northern oceans: Driving the sea surface temperature. *J. Phys. Oceanogr.*, **22**, 859-881.
- Cayan, D. R., and R. H. Webb, 1992: El Niño/Southern Oscillation and streamflow in the western United States. In *El Niño: Historical and Paleoclimatic Aspects of the Southern Oscillation*, Eds. H. F. Diaz, and V. Markgraf, Cambridge University Press, pp. 29-69.
- Charney, J. G., and J. G. DeVore, 1979: Multiple flow equilibria in the atmosphere and blocking. *J. Atmos. Sci.*, **36**, 1205-1216.
- Cheng, X., and J. M. Wallace, 1993: Cluster analysis of the Northern Hemisphere wintertime 500-hPa height field: Spatial patterns. *J. Atmos. Sci.*, **50**, 2674-2696.
- Corti, S., and T. N. Palmer, 1997: Sensitivity analysis of atmospheric low-frequency variability. *Quart. J. Royal Meteor. Soc.*, in press.
- Deser, C., and M. L. Blackmon, 1995: On the relationship between tropical and North Pacific sea surface temperature variations. *J. Climate*, **8**, 1677-1680.
- Dettinger, M. D., and D. R. Cayan, 1992: Climate-change scenarios for the Sierra Nevada, California, based on winter atmospheric-circulation patterns. *Proc. American Water Resources Symposium on Managing Water Resources During Global Change*, Reno, Nevada, pp. 681-690.
- Dettinger, M. D., M. Ghil, and C. L. Keppenne, 1995: Interannual and interdecadal variability in United States surface-air temperatures, 1910–87. *Climatic Change*, **31**, 35-66.

- Dole, R. M., and N. M. Gordon, 1983: Persistent anomalies of the extratropical Northern Hemisphere winter time circulation: geographical distribution and regional persistence characteristics. *Mon. Wea. Rev.*, **111**, 1567-1586.
- Dole, R. M., 1986: Persistent anomalies of the extratropical Northern Hemisphere wintertime circulation: Structure. *Mon. Wea. Rev.*, **114**, 178-207.
- Fukunaga, K., and L. D. Hostetler, 1975: The estimation of the gradient of a density function. *IEEE Trans. Info. Thy.*, **IT-21**, 32-40.
- Gershunov, A., and T. Barnett, 1997: ENSO influence on intraseasonal extreme rainfall and temperature frequencies in the contiguous US: Observations and model results. *J. Climate*, in press.
- Hannachi, A., and B. Legras, 1995: Simulated annealing and weather regimes classification. *Tellus*, **47A**, 955-973.
- Horel, J. D., and J. M. Wallace, 1981: Planetary-scale atmospheric phenomena associated with the Southern Oscillation. *Mon. Wea. Rev.*, **109**, 813-829.
- Horel, J. D., and C. R. Mechoso, 1988: Observed and simulated intraseasonal variability of the wintertime planetary circulation. *J. Climate*, **1**, 582-599.
- Hughes, J. P., D. P. Lettenmaier, and P. Guttorp, 1993: A stochastic approach for assessing the effect of changes in regional circulation patterns on local precipitation. *Water Resour. Res.*, **29**, 3303-3315.
- IMSL Stat/Library, 1991: IMSL Inc., Houston, 1578pp.
- Kimoto, M., 1989: Multiple Flow Regimes in the Northern Hemisphere Winter. Ph.D. thesis, University of California, Los Angeles, CA, 210pp.

- Kimoto, M., and M. Ghil, 1993a: Multiple flow regimes in the Northern Hemisphere winter. Part I: Methodology and hemispheric regimes. *J. Atmos. Sci.*, **50**, 2625-2643.
- Kimoto, M., and M. Ghil, 1993b: Multiple flow regimes in the Northern Hemisphere winter. Part II: Sectorial regimes and preferred transitions. *J. Atmos. Sci.*, **50**, 2645-2673.
- Kimoto, M., M. Ghil, and K.-C. Mo, 1991: Spatial structure of the extratropical 40-day oscillation. In *Proc. 8th Atmos. & Oceanic Waves & Stability Conf.*, American Meteorological Society, Boston, MA, pp. J17-J20.
- Kumar, A., and M. P. Hoerling, 1997: Interpretation and implications of observed inter-El Niño variability. *J. Climate*, **10**, 83-91.
- Legras, B., and M. Ghil, 1985: Persistent anomalies, blocking and variations in atmospheric predictability. *J. Atmos. Sci.*, **42**, 433-471.
- MacQueen, J. (1967): Some methods for classification and analysis of multivariate observations. *Proc. Fifth Berkeley Symposium on Mathematical Statistics and Probability*, University of California Press, Berkeley, pp. 281-297.
- Michelangeli, P. A., R. Vautard, and B. Legras, 1995: Weather regimes: Recurrence and quasi-stationarity. *J. Atmos. Sci.*, **52**, 1237-1256.
- Miyakoda, K., C. T. Gordon, R. Caverly, W. F. Stern, J. Sirutis and W. Bourke, 1983: Simulation of a blocking event in January 1977. *Mon. Wea. Rev.*, **111**, 846-869.
- Mo, K. C., and M. Ghil, 1988: Cluster analysis of multiple planetary flow regimes. *J. Geophys. Res.*, **93D**, 10927-10952.

- Mo, K. C., J. R. Zimmerman, E. Kalnay, and M. Kanamitsu, 1991: A GCM study of the 1988 United States drought. *Mon. Wea. Rev.*, **119**, 1512-1532.
- Molteni, F., S. Tibaldi and T. N. Palmer, 1990: Regimes in the wintertime extratropical circulation. I: Observational evidence. *Q. J. Roy. Meteorol. Soc.*, **116**, 31-67.
- Molteni, F., L. Ferranti, T. N. Palmer, and P. Viterbo, 1993: A dynamical interpretation of the global response to equatorial Pacific SST anomalies. *J. Climate*, **6**, 777-795.
- Namias, J., and D. Cayan, 1984: El Niño implications for forecasting. *Oceanus*, **27**, 40-45.
- Palmer, T. N., 1993: Extended-range prediction and the Lorenz model. *Bull. Amer. Meteor. Soc.*, **74**, 49-65.
- Palmer, T. N., and D. L. T. Anderson, 1994: The prospects for seasonal forecasting—A review paper. *Quart. J. Roy. Meteor. Soc.*, **120**, 755-974.
- Plaut, G., and R. Vautard, 1994: Spells of low-frequency oscillations and weather regimes in the northern hemisphere. *J. Atmos. Sci.*, **51**, 210-236.
- Press, W. H., B. P. Flannery, S. A. Teukolsky, and W. T. Vetterling, 1992: *Numerical Recipes, in FORTRAN*, Second Edition, Cambridge University Press, New York, 702 pp.
- Rheinhold, B. B., and R. T. Pierrehumbert, 1982: Dynamics of weather regimes: Quasi-stationary waves and blocking. *Mon. Wea. Rev.*, **110**, 1105-1145.
- Robertson, A. W., and W. Metz, 1990: Transient-eddy feedbacks derived from linear theory and observations. *J. Atmos. Sci.*, **47**, 2743-2764.

- Ropelewski, C. F., and M. S. Halpert, 1987: Global and regional scale precipitation associated with El Niño/Southern Oscillation. *Mon. Wea. Rev.*, **115**, 1606-1626.
- Ropelewski, C. F., and M. S. Halpert, 1996: Quantifying Southern Oscillation-precipitation relationships. *J. Climate*, **9**, 1043-1059.
- Smyth, P., M. Ghil, and K. Ide, 1997: Multiple regimes in northern hemisphere height fields via mixture model clustering. *J. Atmos. Sci.*, submitted.
- Tibaldi, S., and F. Molteni, 1990: On the operational predictability of blocking. *Tellus*, **42A**, 343-365.
- Vautard, R., 1990: Multiple weather regimes over the North Atlantic. Analysis of precursors and successors. *Mon. Wea. Rev.*, **118**, 2056-2081.
- Vautard, R., and B. Legras, 1988: On the source of low frequency variability. Part II: Nonlinear equilibration of weather regimes. *J. Atmos. Sci.*, **45**, 2845-2867.
- Vautard, R., K. C. Mo and M. Ghil, 1990: Statistical significance test for transition matrices of atmospheric Markov chains. *J. Atmos. Sci.*, **47**, 1926-1931.
- Wallace, J. M., and D. S. Gutzler, 1981: Teleconnections in the potential height field during the Northern Hemisphere winter. *Mon. Wea. Rev.*, **109**, 784-812.
- Wilson, L. L., D. P. Lettenmaier, and E. Skyllingstad, 1992: A multiple stochastic daily precipitation model conditional on large-scale atmospheric circulation patterns. *J. Geophys. Res.*, **97**, 2791-2809.
- Zorita, E., J. P. Hughes, D. P. Lettemaier, and H. von Storch, 1995: Stochastic characterization of regional circulation patterns for climate model diagnosis and estimation of local precipitation. *J. Climate*, **8**, 1023-1042.

Table 1: Stations used in the eight regional time series.

	Station	Location	Elevation (feet)
Central Sierra	Hetch Hetchy	(120°W, 38°N)	1180
	Nevada City	(121°W, 39°N)	847
	Sacramento	(121°W, 38.5°N)	24
	Tahoe City	(120°W, 39°N)	1899
Carson-Truckee	Boca	(120°W, 39.5°N)	1701
	Portola	(120.5°W, 40°N)	1478
	Sierraville	(120.5°W, 39.5°N)	1518
	Tahoe City	(120°W, 39°N)	1899
	Carson City	(120°W, 39°N)	1417
	Reno	(120°W, 39.5°N)	1341
Gunnison River	Cortez	(108.5°W, 37.5°N)	1893
	Durango	(108°W, 37.5°N)	2012
	Grand Junction	(108.5°W, 39°N)	1451
	Gunnison	(107°W, 38.5°N)	2335
	Montrose	(108°W, 38.5°N)	1777
	Ouray	(107.5°W, 38°N)	2390
Rio Grande	Chama	(106.5°W, 37°N)	2393
	Cimarron	(105°W, 36.5°N)	2393
	Durango	(108°W, 37.5°N)	2012
	Gunnison	(107°W, 38.5°N)	2335
	Hermit	(107°W, 38°N)	2743
	Ignacio	(107.5°W, 37°N)	1969
Salt River	Buckeye	(112.5°W, 33.5°N)	265
	Clifton	(109.5°W, 33°N)	1055
	Mc Nary	(110°W, 34°N)	2231
	Miami	(111°W, 33.5°N)	1085
	Roosevelt	(111°W, 34°N)	674
	Springerville	(109.5°W, 34°N)	2152
Virgin River	Beaver	(112.5°W, 38.5°N)	1811
	Caliente	(114.5°W, 37.5°N)	1341
	Milford	(113°W, 38.5°N)	1533
	Orderville	(112.5°W, 37.5°N)	1664
	St George	(113.5°W, 37°N)	841
	Zion Natl. Park	(113°W, 37°N)	1234
Western	Buckley	(112°W, 47°N)	210
Washington	Cedar Lake	(112°W, 47.5°N)	475
	Palmer	(122°W, 47.5°N)	280

	Puyallup	(122.5°W, 47°N)	15
	Snoqualmie Fall	(122°W, 47.5°N)	134
Yellowstone	Lake Yellowstone	(120°W, 44.5°N)	2368
River	Tower Falls	(120°W, 45°N)	1911
	Yellowstone Natl. Park	(120°W, 45°N)	1890
	Island Park	(120°W, 44.5°N)	1917
	Hebgen Dam	(120°W, 45°N)	1978
	West Yellowstone	(120°W, 44.5°N)	2030

Table 2: A comparison of the PDF regimes with weather regimes documented in the literature.

Regime no.	Description	Correlation between PDF and K -means regimes	Corresponding regime found in other studies	
			KG	MVL
1	“El Niño”	0.94	–	–
2	PNA	0.92	1	2
3		0.63	3 & 4	1
4	Reverse-PNA	0.85	2	3
5	Ω -Block	0.95	6	–
6	“La Niña”	0.98	5	–

Key: KG–Kimoto and Ghil (1993b), MVL–Michelangeli et al. (1995). Column 3 gives the pattern correlations between regimes identified using PDF bump-hunting and K -means methods (see text for details). The association of Regimes 1 and 6 with warm and cold events in the tropical Pacific is described in section 6.

Figure Captions

Figure 1: Geographical locations of stations that comprise the eight regional time series.

The Carson-Truckee and Central Sierra time series have the Tahoe City station in common, while the Rio Grande and Gunnison River time series have the Gunnison and Durango stations in common.

Figure 2: Maps of the cross-correlations between December-to-February (DJF) means of local temperature and of DJF gridded 700-mb heights over the North-Pacific–North-American sector. (a) Yellowstone River, (b) Central Sierra, and (c) Salt River. Contour interval is 0.1, negative correlations dashed.

Figure 3: As Fig. 2, but for local DJF precipitation in the three regions.

Figure 4: North-Pacific–North-American weather regimes, constructed using the PDF bump-hunting method. Each map is a composite of hemispheric low-pass filtered 700-mb heights on days belonging to that regime; units are geopotential meters (gpm) and the contour interval is 10 gpm. The regimes are ranked according their respective local PDF maximum, and contain 235, 206, 185, 181, 151, and 156 days respectively.

Figure 5: Frequency of days belonging to each regime for which local daily-average temperatures are above the climatological median, expressed as deviations (%) from the expected 50%. Error bars denote the 95% confidence interval, based on randomly reshuffling the 4140 days 1000 times.

Figure 6: Frequency of extreme warm and extreme cold days: (i) days belonging to each regime for which local daily-maximum temperatures are above the climatological 90th percentile (Δ) and, (ii) days for which daily-minimum temperatures are below the 10th percentile (\ominus); both expressed as deviations (%) from the expected 10%.

Error bars denote the 95% confidence interval, based on randomly reshuffling the 4140 daily-maximum temperatures 1000 times.

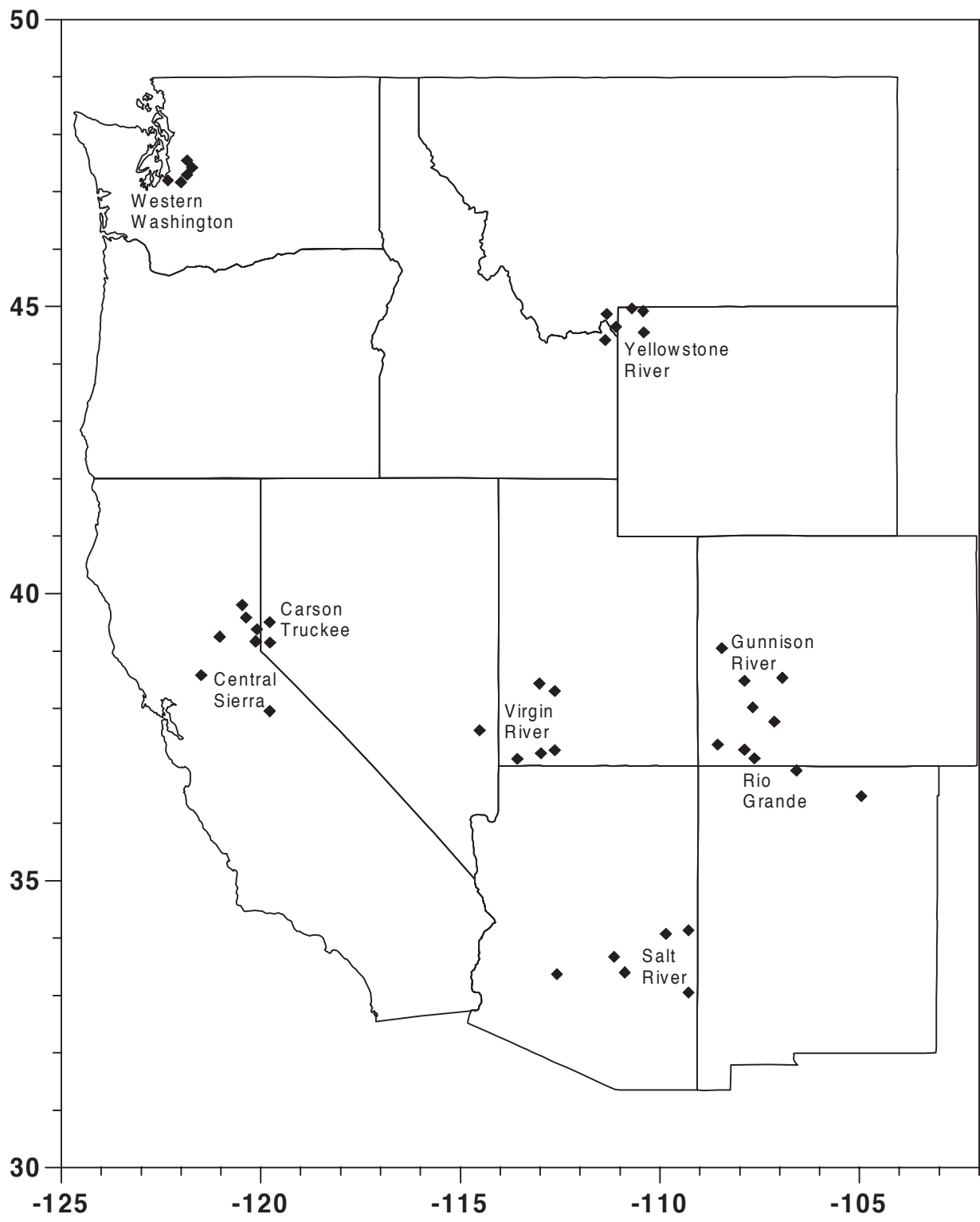
Figure 7: Frequency of days belonging to each regime on which precipitation was recorded, expressed as deviations (%) from the 46-winter climatological frequency. The total number of days with recorded precipitation is given in the top left-hand corner. Details as in Fig. 5.

Figure 8: Differences in regime frequency (days/winter) for locally warm-minus-cold winters (circles) and wet-minus-dry ones (diamonds) (see text). Error bars indicate the 90% confidence interval, based on random reshuffling the 46 winters (temperatures) 1000 times.

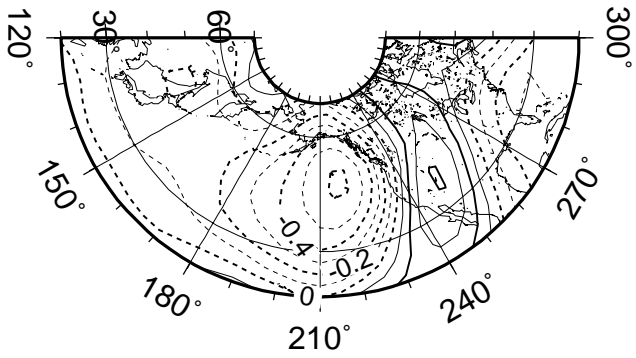
Figure 9: Regime frequency (days/winter) for (a) El Niño, and (b) La Niña winters, defined by deviations of the Southern Oscillation index (SOI) exceeding one standard deviation. Error bars indicate the 95% confidence interval, based on random reshuffling the 46 winters 1000 times.

Figure 10: Composites of SST anomalies for winters in which regime frequency exceeds the 80th percentile of the 46-winter frequency distribution. The number of winters selected for each regime is given in parentheses. Contour interval is 0.2K, negative and zero contours are dashed. Stippling denotes statistical significance according to a two-tailed Student *t*-test at the 95% level. (a) Regime 1: the DJF winters are 1952, 1957, 1959, 1965, 1968, 1969, 1977, 1982, 1986, and 1991, where the year in which the winter starts is given. (b) Regime 2: 1957, 1967, 1969, 1973, 1976, 1977, 1980, 1984, 1985, and 1989. (c) Regime 3: 1951, 1958, 1964, 1966, 1971, 1974, 1978, 1987, 1988, 1989, and 1991. (d) Regime 4: 1949, 1951, 1956, 1958, 1970, 1971, 1981, 1984, 1990, and 1992. (e) Regime 5: 1951, 1956, 1961, 1962,

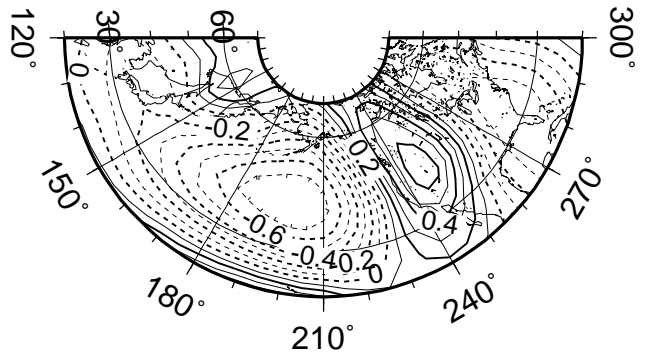
1971, 1973, 1977, 1980, 1981, 1983, 1990, and 1992 (f) Regime 6: 1950, 1952, 1955, 1961, 1967, 1970, 1980, 1984, 1985, and 1993.



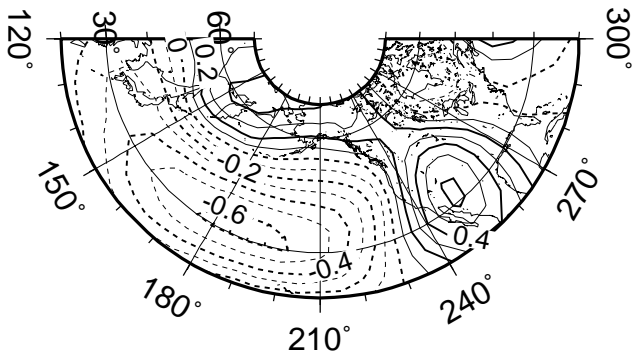
a) Yellowstone River



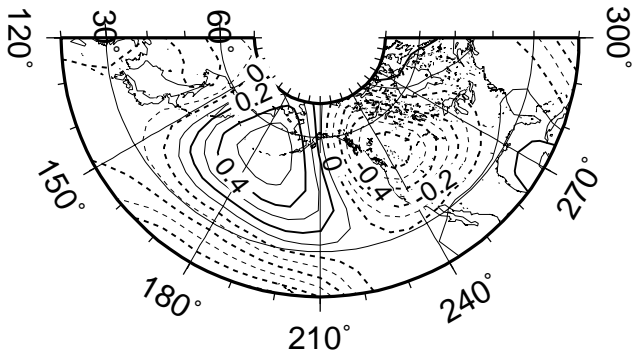
b) Central Sierra



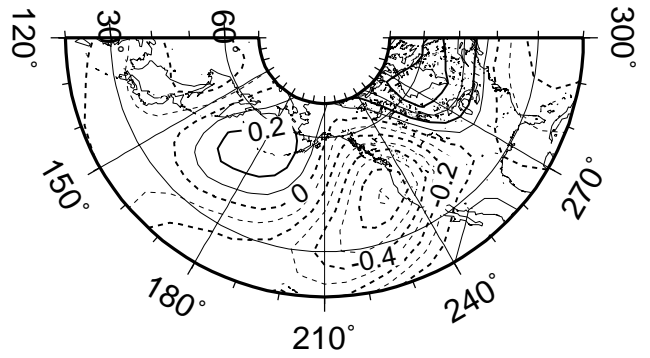
c) Salt River



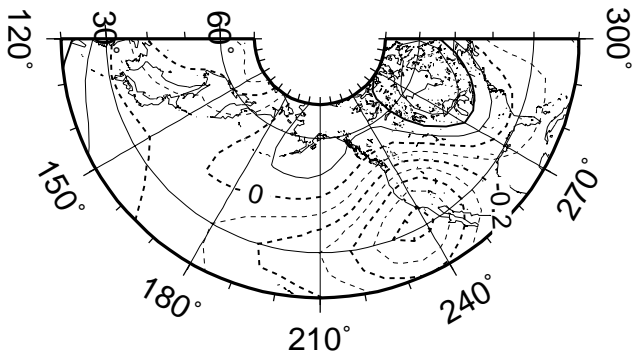
a) Yellowstone River

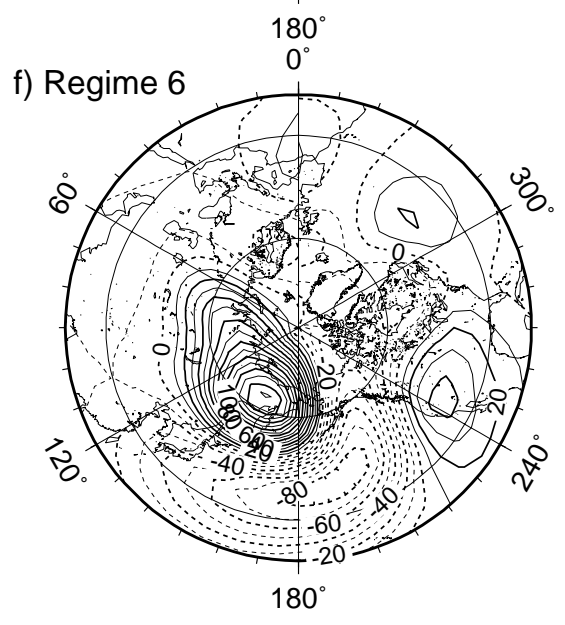
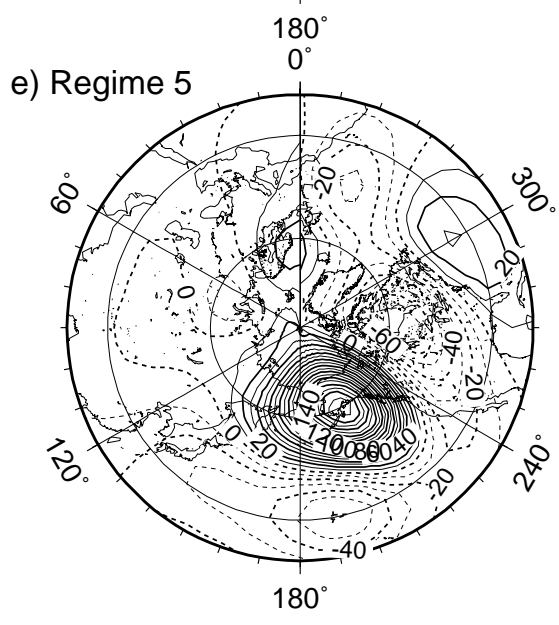
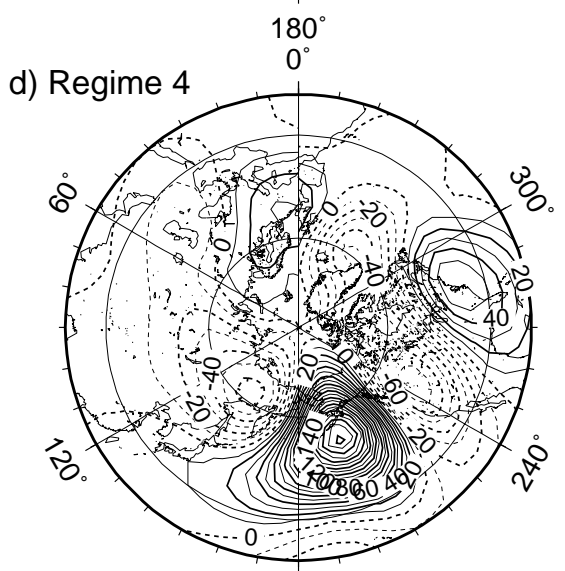
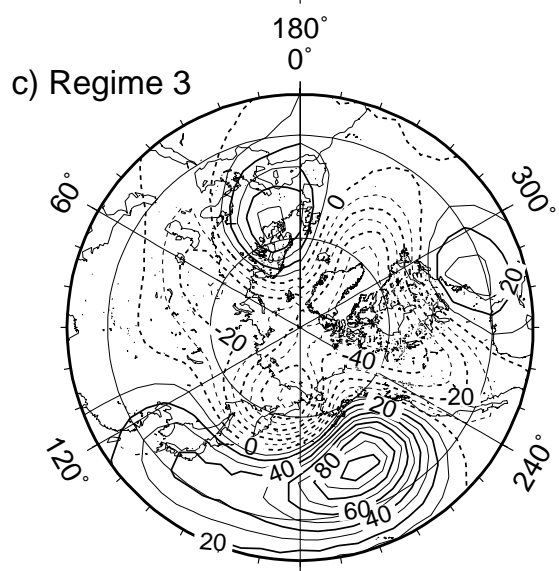
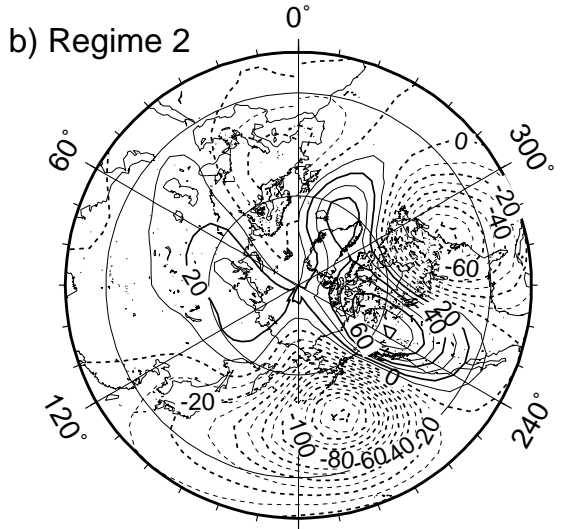
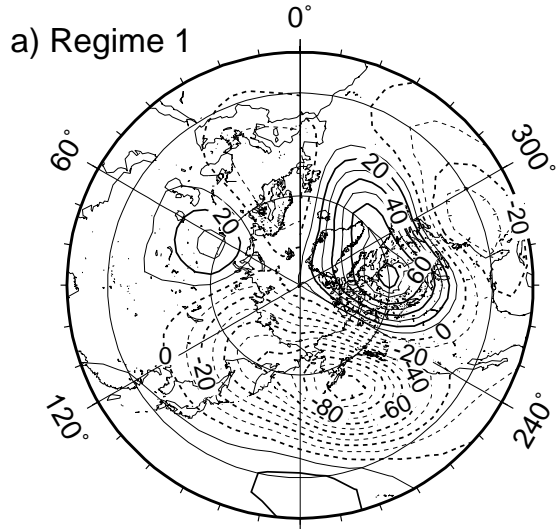


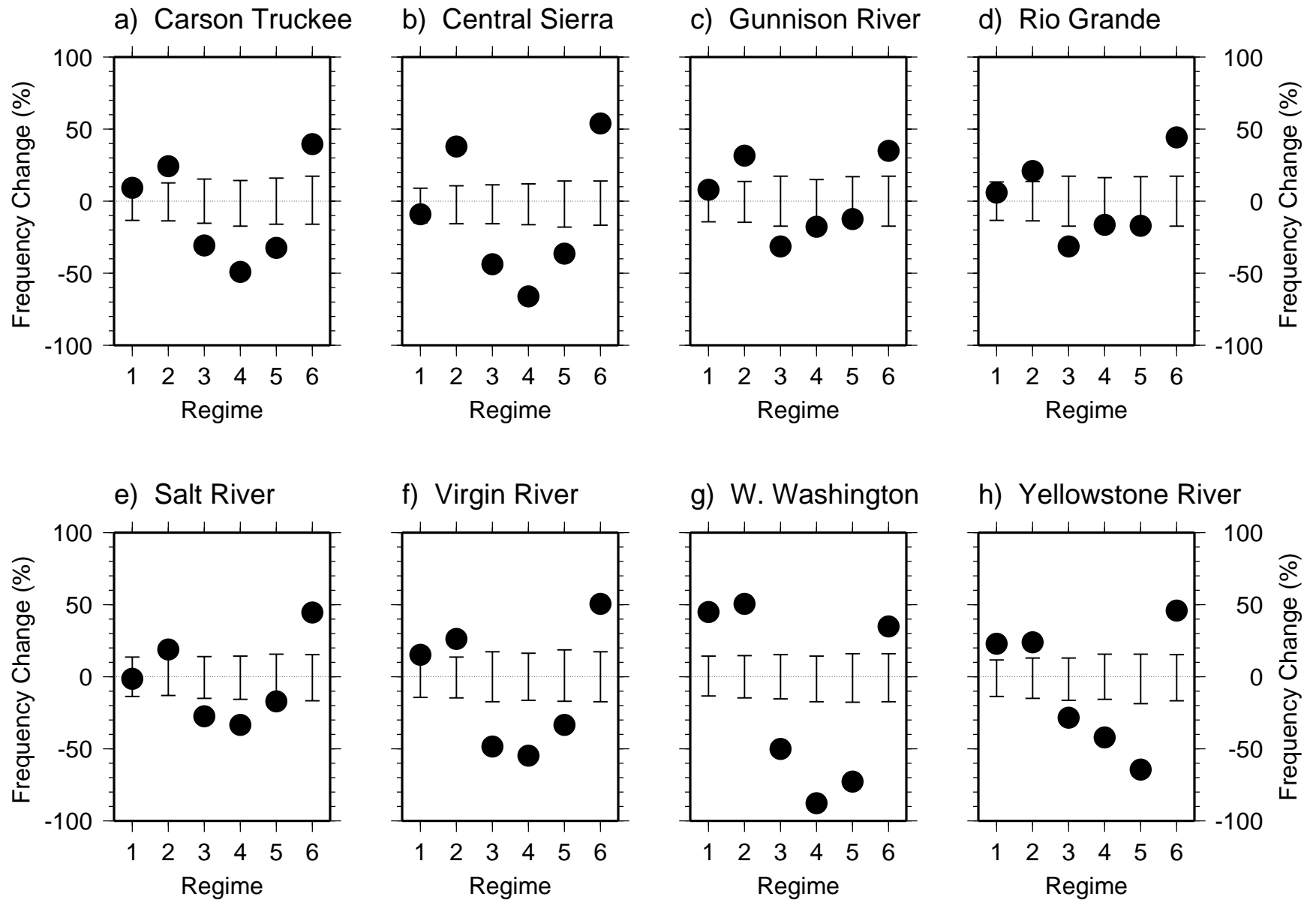
b) Central Sierra

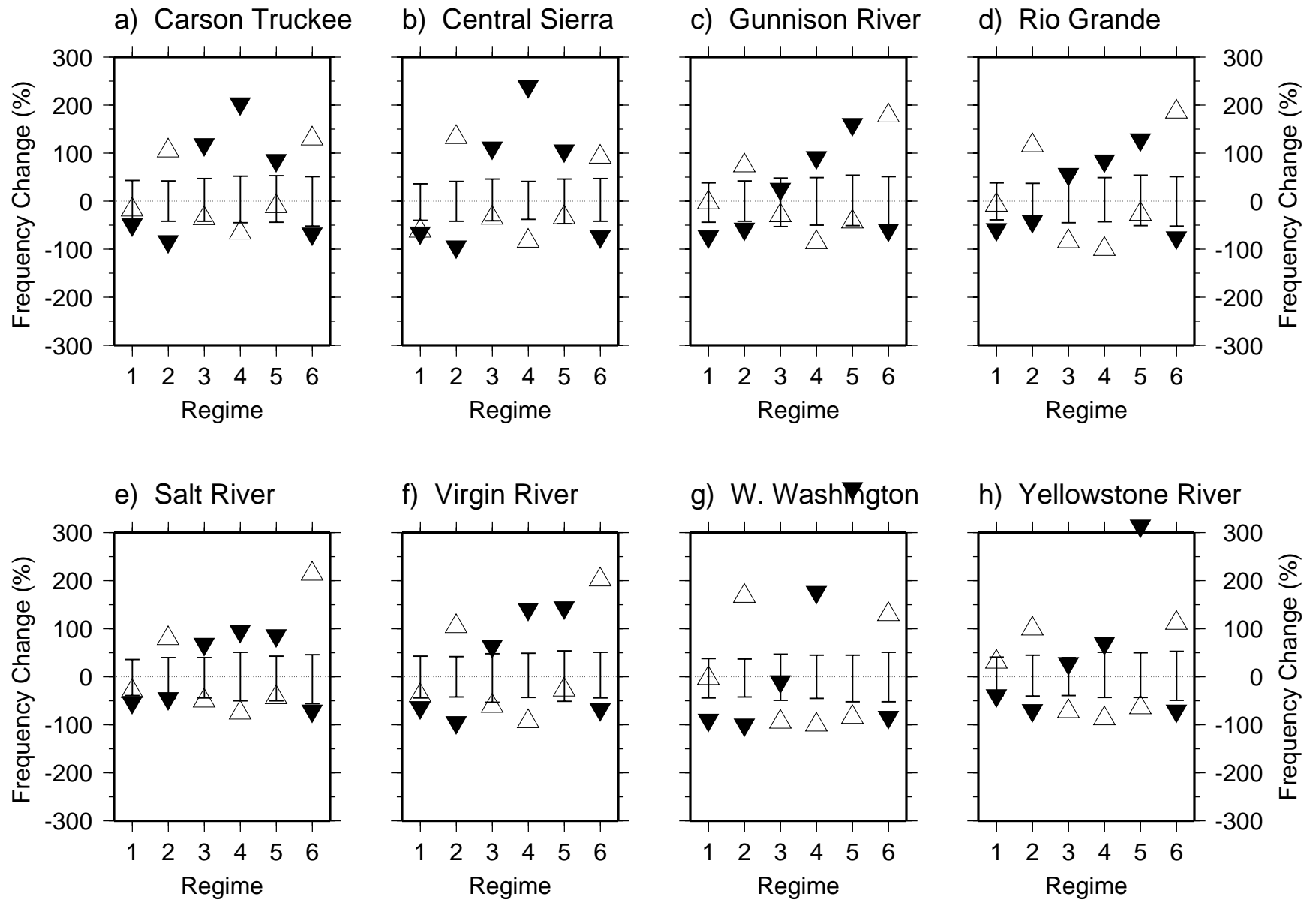


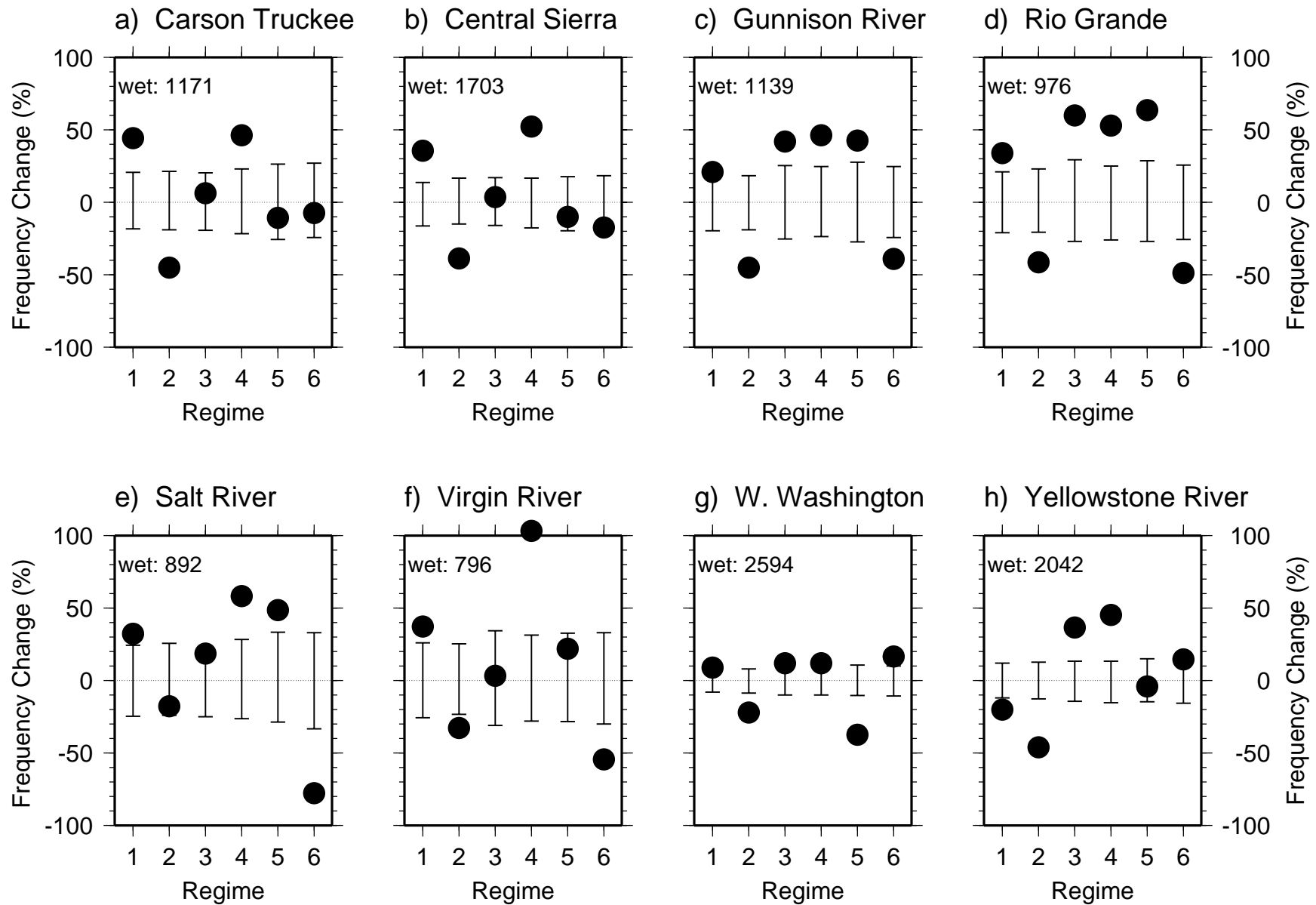
c) Salt River

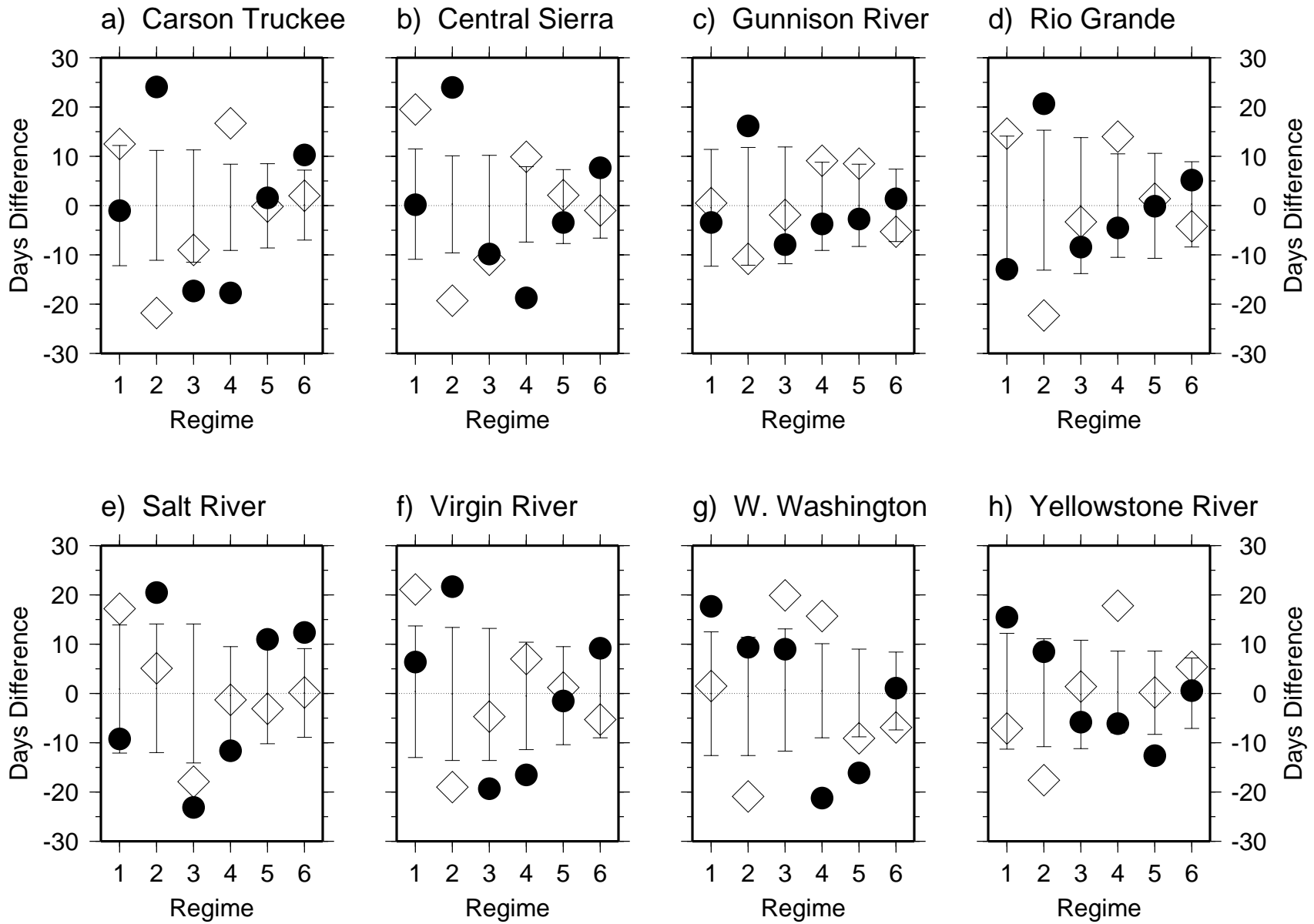


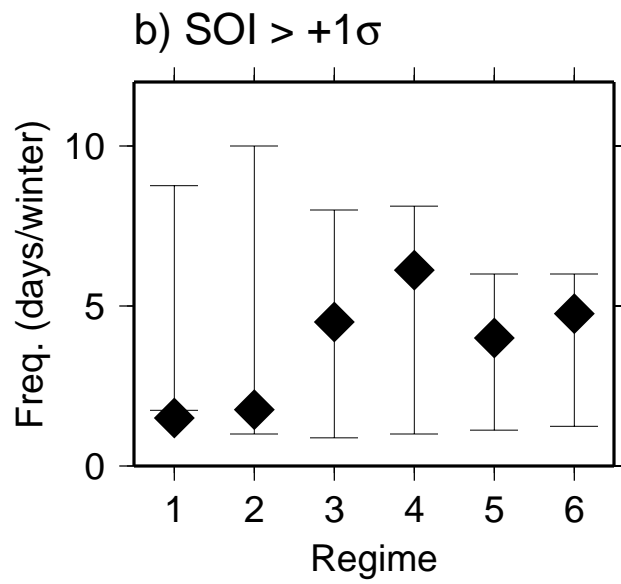
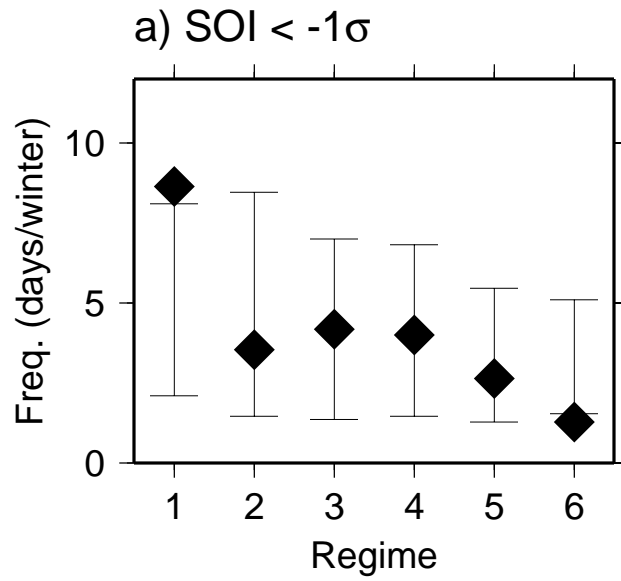




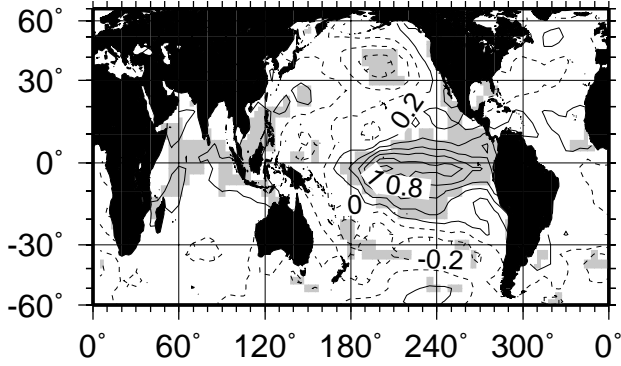




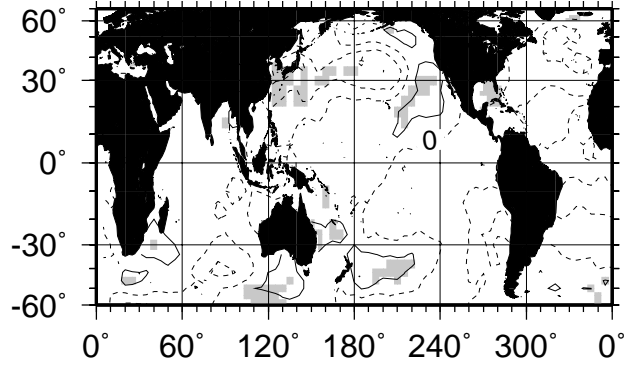




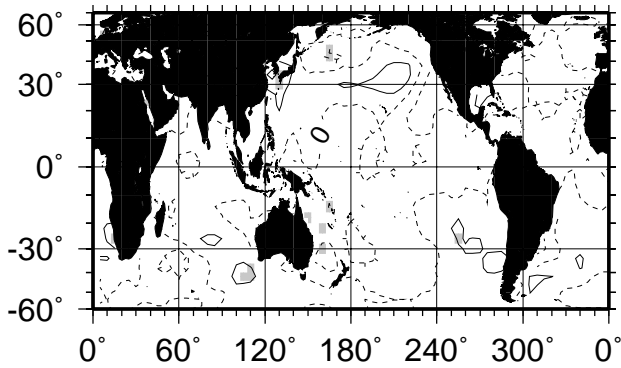
a) Regime 1 (10)



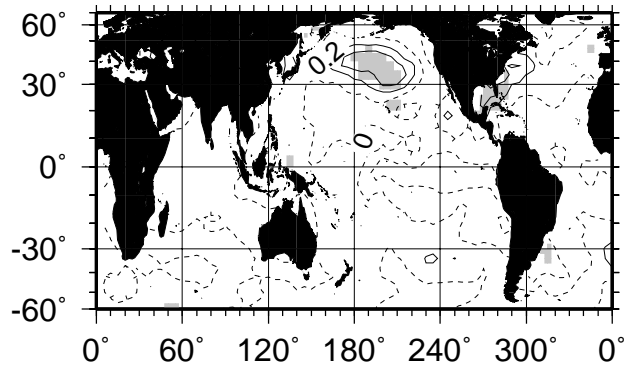
b) Regime 2 (10)



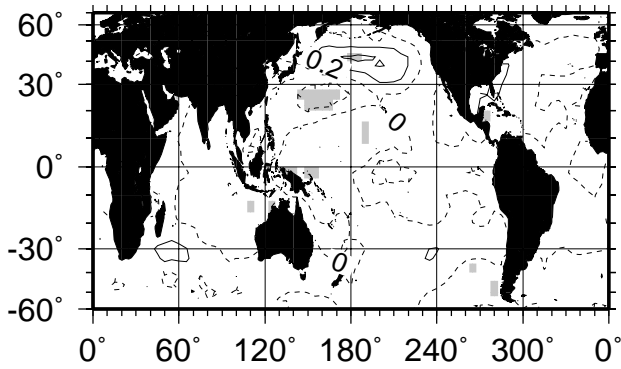
c) Regime 3 (11)



d) Regime 4 (11)



e) Regime 5 (12)



f) Regime 6 (10)

